Copper micro-electrode fabrication using laser printing and laser sintering processes for on-chip antennas on flexible integrated circuits

O. Koritsoglou,[1] I. Theodorakos,[1] F. Zacharatos,[1] M. Makrygianni,[1] D. Kariyapperuma,[2] R. Price,[2] B. Cobb,[2] S. Melamed,[3] A. Kabla,[3] F. de la Vega,[3] and I. Zergioti[1,*]

[1]*National Technical University of Athens, Physics Department, Iroon Polytehneiou 9, 15780, Zografou, Athens, Greece*
[2]*PragmatIC, 400 Cambridge Science Park Milton Road, Cambridge, CB4 0WH, UK*
[3]*PV Nano Cell Ltd., 8 Hamasger St., P.O. Box 236, Migdal Ha'Emek, 2310102, Israel*
[*]zergioti@central.ntua.gr

Abstract: Recent advances in flexible electronics have highlighted the importance of high throughput, digital additive microfabrication techniques. In this work, we demonstrate the combination of laser printing and laser sintering of a novel copper nanoparticle ink onto flexible substrates in order to produce oxide free conductive copper patterns in ambient atmospheric conditions. The printed patterns exhibit high reproducibility, very low resistivity (about 2x bulk), and negligible oxidation according to Raman spectroscopy. The process has been employed for the fabrication of an on-chip antenna on a flexible substrate for use in combination with a flexible circuit, in applications where a small form factor and simplicity of integration are required alongside ultra-low cost, e.g. consumable tagging.

1. Introduction

The field of flexible and stretchable electronics has evolved very rapidly over the past 10 years, enabling unprecedented innovations in consumer electronics [1] and sensors [2]. As the demand for miniaturization and power of flexible devices increases, so does the need for novel manufacturing processes and materials. The substrates of flexible components are incompatible with conventional manufacturing techniques and require alternative microfabrication approaches. One of the most widely used additive micro-manufacturing technologies relies on the direct printing followed by selective sintering of metal nanoparticle inks. Laser printing relying on the Laser Induced Forward Transfer (LIFT) technique, combined with selective laser sintering stand out among the additive micro-manufacturing technologies [3–5] owing to the high speed (>1 m/s) and high resolution (<50 µm) [6], as well as the lateral selectivity and minimized heat affected zone with demonstrations of highly conductive micro-patterns in flexible electronic applications [7–11]. In this technology, inks comprising metals like gold and silver have been primarily employed due to their high conductivity and environmental stability [12]. Despite their excellent behavior, these noble materials are costly and thus not well suited to the target range of applications.

Copper, having high conductivity and much lower price, can be an attractive candidate for loading solution processed metal nanoinks. However, copper nanoparticle inks tend to oxidize quickly in ambient conditions, at an increasing rate in high temperatures (>150 °C), which are essential for the successful sintering of the inks. So far, numerous studies have been dedicated to addressing this issue: the very first attempts to prevent the oxidization of the copper nanoinks, relied on oven sintering in reducing atmosphere [13–16]. In 2007, B. Park et al. [13] inkjet printed copper nanoparticle inks onto glass substrates and using a vacuum furnace at 325 °C,

achieved a resistivity of 17.2 μΩ·cm. In 2010, Yabuki et al. [14] achieved a resistivity of about 20 μΩcm using a furnace with nitrogen and hydrogen-argon mixed gas at 300 °C. In the same year, Kim et al. [15] lowered the resistivity down to 4 μΩ·cm, by adding alcohol and formic acid as reduction agents in the nitrogen gas flow, and Joo et al. [16] in 2012, printed and sintered in a nitrogen gas flow furnace, a copper nanoink onto a flexible polyimide substrate, with resulting resistivity of about 13 μΩ·cm. Unfortunately, the majority of flexible substrates, which are thermoplastics like PEN or PET, have low glass transition and melting temperatures and consequently they can't be exposed to temperatures in the order of 200–300 °C in a furnace. Thus, alternative methods of sintering had to be employed in order to fabricate conductive patterns, such as chemical [17] and photonic sintering [18–30].

There are two different approaches in photonic sintering, flash light and laser sintering. Flash light sintering can cover a very large area of the printed substrate with a single pulse, offering no lateral selectivity and the resulting heat affected zone might be extended. Flash light sintering of copper nanoparticle inks has been studied thoroughly in the last decade [18–23], with the best resistivity value (5 μΩ·cm), achieved from H-S. Kim et al. [23], in 2009. On the other hand, laser pulses are spatially confined in a small area, and the sintering process is performed by scanning the laser beam over the printed pattern. The utilization of short and ultra-short laser pulses, minimizes the heat affected zone to the order of less than 1 μm, and by employing state of the art galvo-scanning systems, scanning speeds higher than 1 m/s can be readily achieved, offering high throughput and high lateral resolution and at the same time laser pulse intensity can be adjusted according to the requirements of each pattern. The last few years, the laser sintering of copper nanoparticle inks has been extensively studied [24–30] as well, and the impressive resistivity value of 5.13 μΩ·cm, has been demonstrated by Zenou et al. [30], using a CW laser at 532 nm, in 2014. In 2015, Niittynen et al. [31] conducted a comparative study between flash light and laser sintering on inkjet printed copper nanoparticle layers, resulting in a resistivity less than 8.55 μΩ·cm for both sintering techniques, with laser sintering providing slightly better results.

To date, a number of commercial demonstrations of copper nanoparticle inks exist, developed mainly for screen and inkjet printing techniques [32,33]. Among them, NovaCentrix (HQ in Texas, USA) synthesized an ink composed of submicron particles of copper formate, a copper precursor that has a self-reduction property for achieving sintering of copper interconnections on plastic substrates with intense pulsed light curing. Copprint (HQ in Jerusalem Israel) synthesizes printable copper inks compatible with standard sintering process (avoiding photonic or laser sintering), involving heating the printed pattern for a few seconds in a standard office laminator for sintering. However, to our knowledge, none of the above inks and pastes are optimized for laser printing, and some of the inks contain copper oxide and copper formate as a precursor instead of copper, which are less effective for thick patterns and high throughput.

Flexible integrated circuits for RFID applications have been explored using a variety of materials and substrates. Digital circuits for this application, however, have exclusively focused on fabrication of a thin film transistor-based RFID circuit on a separate substrate from an antenna, with an additional assembly step required to attach them via a conductive adhesive [34]. Meanwhile in traditional silicon based CMOS integrated circuits, on-chip antennas have received attention for a variety of applications such as biosensors [35] and asset tagging [36].

Having recently demonstrated for the first time in literature the high speed laser printing and laser sintering of Ag NP micropatterns in a fully digital process [11], in this work we report on the efficiency of laser printing combined with laser sintering for an oxidation free fabrication of conductive Cu patterns. A novel Cu ink synthesized especially for laser printing and laser sintering, with high metal content (60%), high viscosity (~430 kcP at 1 s^{-1}) and optimized composition (additives, solvent), enables the accomplishment of the lowest resistivity reported in the literature for laser sintering of Cu nanoinks: 3.3 μΩ.cm (~2xbulk). We employ Raman spectroscopy and EDX analysis to prove that pristine Cu ink and ink dried in ambient atmosphere

show a high degree of oxidation, whereas after laser sintering, the resulting micropatterns are oxide free. Furthermore, the potential of the reported technology for the additive manufacturing of flexible electronic devices is demonstrated by the successful digital fabrication of a spiral loop meeting the design rule and electrical conductivity requirements to make an antenna for near-field applications at a size compatible with an effective total solution cost.

2. Methods and experimental configurations

2.1. Materials

2.1.1. Copper Np ink synthesis and customization for laser sintering

A nanoparticle copper ink based on Sicrys particles was developed for this work especially for laser printing and laser sintering. The ink development included optimization of the type of solvent, metal concentration, and rheological characteristics for optimum printing and sintering.

The nano copper ink is based on Sicrys single crystal particles, as confirmed by electron backscatter diffraction (EBSD) technique, and demonstrated by the geometrical crystals observed by TEM (see Fig. 6(b), Appendix). It is hypothesized that single crystal particles impart exceptional stability and electrical properties to the inks of which they comprise. The procedure used for copper particle synthesis included the following steps: 102 g of $CuCl_2H_2O$ (0.6 mol) and 18.5 g of Polyvinylpyrrolidone (PVP, MW = 55,000) were dissolved in 900 ml de-ionized water in a 3 L vessel (solution A). In parallel, 45 g of $NaBH_4$ were dissolved in 300 ml de-ionized water (solution B). Solution B was gradually introduced into solution A under intensive mechanical stirring (500-600 rpm), forming nano copper particles. Argon was blown into the reaction mixture throughout the procedure, and mild cooling was applied to keep the temperature under 70 °C (the initial temperature was about 25 °C). Solution B was added to solution A until the mixture reached a pH of 5.1, after which the flow of solution B was discontinued, and the reaction mixture was stirred for an additional 10 minutes. The resultant dispersion color was dark-red, with average particle diameter of ~40 nm. The dispersion was purified (washed) in a cross-flow microfiltration system using de-ionized water until no salts could be detected. A high boiling temperature solvent was added to the nano copper aqueous dispersion, and water was distilled off in a Rotavapor system. Different solvents can be employed, and the final copper ink concentration was determined by the corresponding solvent/metal ratio.

The solvent type was chosen according to its surface tension and evaporation rate properties. In this work the solvent diethylene glycol monobutyl ether (DGBE) was selected in order to impart a homogenous donor coating with acceptable wetting and drying rate, as well as printed geometry characteristics, taking into account the wetting properties of the receiving substrate. In addition, it has been shown in [37] that printable LIFT inks require a high viscosity and high shear thinning effect in order to achieve a homogeneous donor formation, followed by stable jets and subsequent reproducible printed patterns. Since ink viscosity is highly influenced by metal concentration, the metal content was raised and fine-tuned to 60% for optimum performance in the DGBE solvent of choice, as well as contributing to the printing process throughput and formation of dense printed patterns.

Rheological properties of the copper nanoparticle ink were measured with Malvern Kinexus Pro+ rotational rheometer. Conditions of measurements included a serrated plate-plate set-up, gap 0.5 mm, temperature 25 °C, sample volume 1.7 ml. According to viscosity-shear rate profile obtained (see Fig. 6(a), Appendix), copper nanoparticle ink exhibits a non-Newtonian behavior with shear-thinning effect. Particle size distribution of Cu dispersions was measured with LUMiSizer® dispersion analyzer.

2.1.2.   Donor and receiver substrates

The donor materials involved in this study were 3inch quartz wafers which show excellent wettability to the coated ink, very high total visible light transmission (>95% at 532 nm) and very low surface roughness (<2 nm). The receiving substrate was an SU8 layer of 450 nm thickness, coated on top of a glass substrate. SU-8 is an epoxy-based photoresist with high chemical and thermal stability (Tg >200 °C when fully crosslinked) [38]. Furthermore, its low cost and excellent optical transparency beyond 400 nm makes it a preferred material for the fabrication of large variety of optoelectronic components.

2.2.   *LIFT and laser sintering: process and setup*

The laser printing process of the copper micro-patterns has been achieved by implementing the LIFT technique at the liquid phase as described in [39], but with proper tuning of certain parameters, so as to optimize the process for high viscosity inks: in this study, no sacrificial layer has been utilized, and the ink layer on the donor substrate (10μm thick) was coated using doctor blade film application. In general, ink layer thickness on donor substrate may vary from a few nm to a few μm, however by decreasing the thickness to a few nm will shorten the processing window, due to the very short drying time of the thin layer. During laser printing, the donor substrate was placed above the receiving substrate at close vertical distance (100 μm) (Fig. 1(a)), and the laser beam was focused on the ink/ donor substrate interface, through the f-theta lens of the galvanometric scanning system described below. The fabrication of patterns, such as lines, on the substrate has been accomplished by scanning the laser beam over the donor surface, creating in this way multiple jets which form overlapping droplets [37].
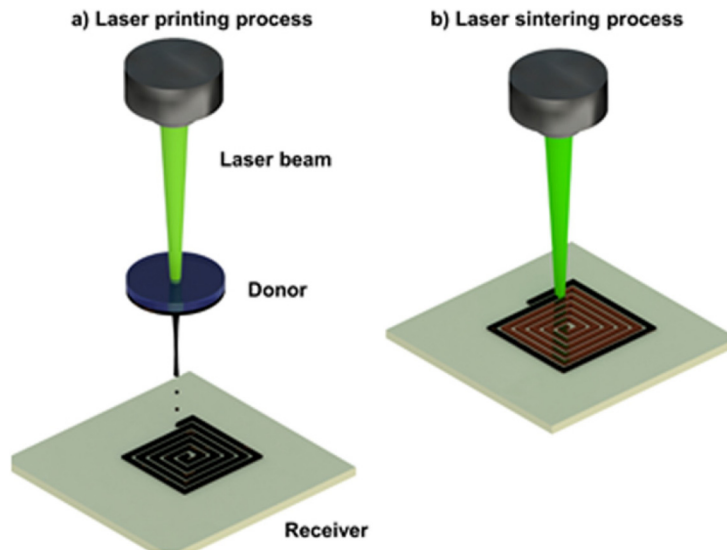

Fig. 1. Schematic illustration of (a) the laser printing and (b) laser sintering of the copper ink.

After the laser printing process is over, a sintering process is required so that the copper ink patterns obtain the desired electrical properties. In this work we have employed laser sintering for selective and high resolution heating of the nanoparticles, as it is extensively described in previous works [9–11]. First the printed ink dries in ambient atmosphere for a few minutes at room temperature, then the sintering procedure takes place with the direct exposure of the pattern

to the laser beam (Fig. 1(b)), which operates at a repetition rate of 60 kHz and a scanning speed of 0.1 m/s.

The printing and sintering processes of the copper ink have been carried out using the experimental configuration described in detail in a previous work [11]. Briefly, the laser source is a pulsed Nd:YAG laser with maximum average output power of 20 W. The laser operates at 532 nm with a pulse duration of 20-200 ns depending on the repetition rate, which can reach up to 500 kHz. In order to scan all over our samples swiftly, we utilize a galvanometer scan head with maximum scanning speed up to 5 m/s, combined with a motorized x-y-z motion system of stages, that enables the movement of the donor and the substrate in relation to one another. The average power of the laser beam is adjusted via a custom made half wave- plate and polarizer based attenuation system.

2.3. Characterization methods

Film profile measurements were carried out with a profilometer (Veeco Dektak 150, tip radius 12.5 μm), with a stylus force of 6.00 mg. Micrographs were taken with an optical microscope (Leica) coupled with a digital camera system (Canon PowerShotS50). For the recording of Raman spectra, micro Raman system (T64000-JY) was used with Argon laser at 514.5 nm. Typical I–V measurements were performed with an HP4140 B pico-amperometer, and the specific resistivity of the laser sintered lines was determined by taking into account the lines' profiles. In addition, scanning electron microscopy (SEM) images and EDX spectra, were obtained using a SEM system (Philips 515 SEM with EDX).

3. Results and discussion

3.1. LIFT of the copper ink

The dependence of the droplet diameter on the laser fluence is shown in Fig. 2(b), in which we can see an optical microscopy image of ink droplets printed using a range of laser fluences from 150 up to 420 mJ/cm^2. In Fig. 2(c) the produced lines of a particular laser fluence (360 mJ/cm^2) at different scanning speeds of the laser beam over the printed pattern (from 0.65 to 0.75 m/s) are displayed. In low laser fluences, the printed droplet has a relatively small diameter, which depends on the laser spot size on the donor. In this case, the laser spot size at the transparent carrier/ink layer interface of the donor substrate is 60 μm. Droplets of this diameter size are printed for a laser fluence of 210 mJ/cm^2, and further decrease of the fluence doesn't result in smaller diameters, as illustrated in Fig. 2(a). As the laser fluence increases, the diameter of the printed droplets increases accordingly, reaching up to 100 μm. Further increase of laser fluence results in distorted droplets with splashes and satellites, thus these energy fluence regimes are not included in this study. The printed droplets in this wide laser fluence processing window of 150-420 mJ/cm^2, are quite uniform with circular shape and the appearance of satellite droplets is rare. Furthermore, the lines are very uniform in a narrow range of scanning speeds, from 0.65 to 0.75 m/s (which corresponds to an overlap between the successive droplets from 28 to 17 percent) and their width is slightly higher than the corresponding diameter of the droplet. The optimal overlap for lines printing using LIFT is dependent on a variety of parameters: the viscosity, the substrate's surface energy and the inks surface tension are all important factors defining the optimal overlap. At higher scanning speeds (up to 0.9 m/s), we can still obtain connected lines, however their width varies remarkably. In this case, there is no overlap between the successive droplets, however the droplets are sufficiently close to each other for capillary forces to connect them. Additionally, if the laser scanning speed drops to less than 0.6 m/s, satellite droplets and debris appear around the printed patterns. Two factors may be responsible for this phenomenon: first, unstable successive jets, which occur when the distance between two consecutive pulses is smaller than a critical value, defined by a plethora of parameters (e.g. laser spot size, laser

fluence, inks properties etc.) [40]; second, jet impact on already printed ink (splashing effect) [41]. In this case, the debris must be attributed mainly to the unstable successive jets as the high viscosity of the ink significantly limits the splashing effect. These printing results, indicate that we can have excellent control over the size and morphology of the printed patterns, factors which are of great importance for the commercialization of the process.
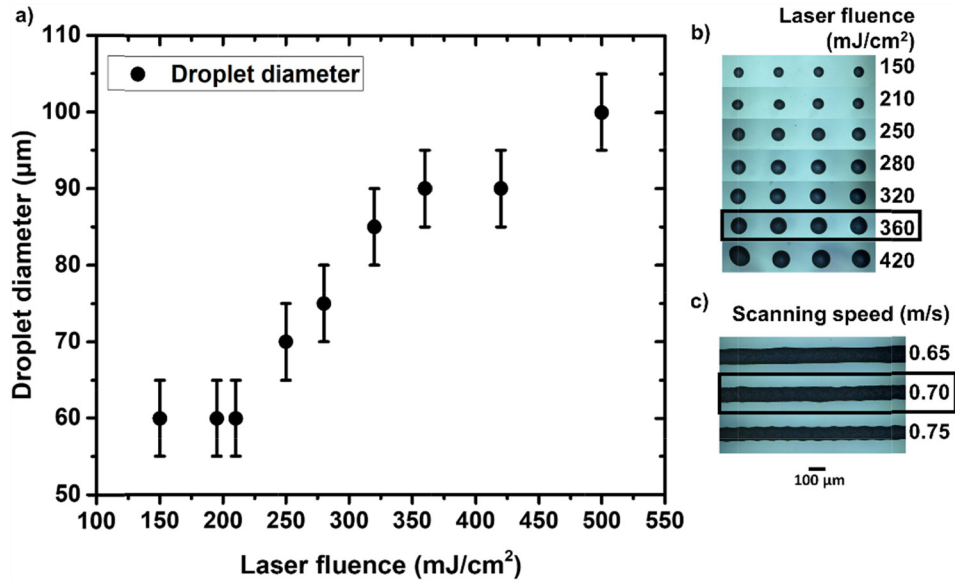

Fig. 2. (a) Diameters of the printed droplets vs printing laser fluence, (b) optical microscopy images of the printed droplets at different laser fuences and (c) of the printed lines utilizing different laser scanning speeds.

The aforementioned printing parameters can be used to print patterns such as pads or wider lines as well. By printing lines with a 70 μm pulse to pulse separation distance and vertical distance between successive lines equal to 50 μm, we formed a wider line with similar quality and height as the single lines produced under the same conditions. This approach was utilized for the printing of the spiral tracks, which are presented in our test case below (section 4).

3.2. Laser sintering and electrical characterization

The laser sintering of the printed patterns was carried out using the same DPSS ns pulsed laser as in the printing process. The profile of the laser beam was Gaussian, hence the laser fluence was calculated at the $1/e^2$ beam width (spot size on samples 100 μm); the thermal damage to the SU8 substrate at the edges of the lines is negligible. As this Cu ink is a novel, research grade material, initially, a sintering process calibration was carried out. Initially, lines of 90 μm width were printed and the process was implemented using a range of laser fluences varying from 200 to 310 mJ/cm², scanning with a single pass at a fixed scanning speed of 0.1 m/sec, which corresponds to horizontal pulse to pulse overlap 98%, according to the parameters applied in previous study [11]. As the laser fluence increases, the resistivity goes down, until the fluence reaches 290 mJ/cm², in which we observed the minimum value. From that point and on, the resistivity increases once again due to the increased thermal loading on the sintered lines and the consequent substantial thermal damage on the substrate [42]. Using single pass scanning, the best electrical resistivity we could obtain, had the value of 56 μΩ·cm. This value is about 30 x the bulk copper resistivity (1.68 μΩ·cm), and although our patterns already indicated metallic behavior,

this value was still far from the goal of this study, which was to achieve optimal conductivity meeting the requirements of high quality factor (Q) RF (or electronic) devices.

In order to improve further the electrical conductivity of the laser printed and laser sintered patterns, a laser scanning study was conducted (on wider lines of about 230 μm): by introducing vertical overlap of the scanning process we investigated the effect of y-scanning step, which corresponds to the vertical distance between the laser spot centers in two successive laser scan passes over the printed pattern. In this way, for the laser fluence of 290 mJ/cm^2 and while keeping the former (horizontal) x-overlap constant, we varied the y-overlap, by varying the scanning in the range of 50 to 5 μm. The results derived from this study are presented in Fig. 3, from which it is evident that for a scanning step of 50 μm, the resistivity already drops significantly from 56 to only 4 μΩ·cm. As we scanned the pattern more densely (with smaller scanning steps), the resistivity kept on improving, and at a scanning step of 5 μm, it reached the impressive value of 3.3 μΩ·cm (∼ 2x bulk resistivity), which outmatches the best reported values in the literature [30]. Side view SEM characterization carried out on laser sintered patterns confirms that sintering has been fully accomplished throughout the copper layer (from top to bottom).
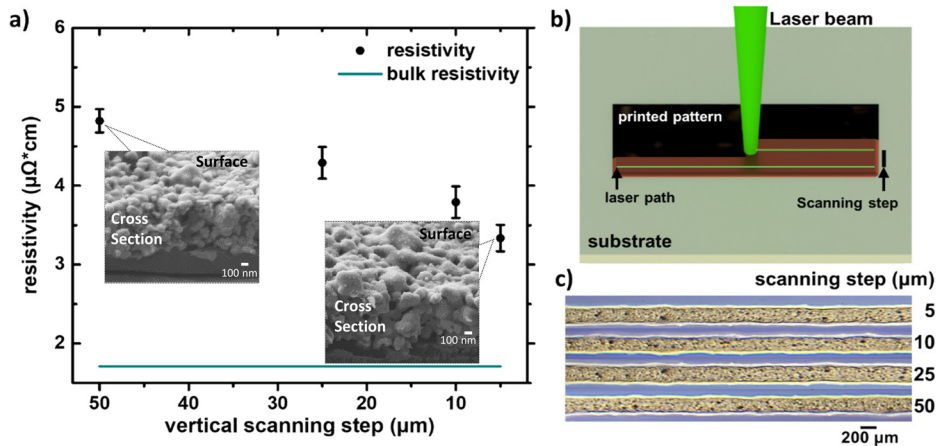

Fig. 3. (a) Resistivity vs vertical scanning step and SEM images indicating that surface morphology is reproduced in the cross-section, confirming efficient in-depth sintering, (b) schematic illustration of the laser sintering process with vertical scanning, (c) optical microscope image of the corresponding sintered lines

The y scanning step does not only define the total amount of energy that is deposited onto the structure, but also its spatial distribution: by carefully tuning the vertical overlap, one can mitigate the effect of the Gaussian profile and achieve a uniform sintering effect. In order to elucidate the contribution of these two factors (total energy and spatial distribution), sintering with laser multi passes without y-canning have also been performed (to 90 μm wide lines for the laser fluence of 290 mJ/cm^2) and even after 100 laser passes the change of the resistivity was insignificant (this behavior is more likely to be attributed to the change of the optical and absorbance properties of the material after the laser illumination). As a result, this set of measurements indicates that the uniformity of the laser energy deposition is an important factor that needs to be considered in the sintering process.

The average height of all the sintered lines was measured with profilometry at 900 ± 50 nm, and the resulting very low resistance indicates that sintering has been accomplished homogeneously throughout the whole thickness of the lines and not superficially, which would result in poor conductivity and line quality. Furthermore, according to the simulations conducted within a previous study of the authors for Ag [11], applying consecutive laser pulses for laser fluences

> 100 mJ/cm^2 at high repetition rates, results in temperature profiles which suffice for efficient sintering (>250 °C), across the whole thickness of the structure. It was shown in particular, that the very high thermal conductivity of Ag, ensures that heat is transferred through hundreds of micrometers vertically, with minor dissipation, within hundreds of nanoseconds, until it reaches the metal/ polymer interface. There the temperature drops very steeply and the heat affected zone into the polymer is in the order of 1 micrometer. In the present study, having a very relevant interface and sintering process parameters, we can expect that laser sintering is achieved throughout the entire Cu structure also, taking into consideration that the thermal conductivity of Cu is only 5% lower than Ag's [43], and optical absorption coefficient of Cu is very high at 532 nm ($\alpha = 8.0996 \times 10^{+5}$ cm^{-1})[44].

Close examination using optical microscopy reveals no evident thermal damage on the substrate owing to the laser processing. Previous studies of the authors [42] have shown that nanosecond pulsed lasers can selectively sinter Ag nanoparticle inks, while inducing minimal thermal damage on low Tg polymer substrates, with a heat affected zone in the order of 1 micrometer. In the present study the thermally damaged zone is expected to be even smaller, as SU8 is a thermally stable polymer with Tg around 200 °C.

3.3. Raman spectroscopy and EDX analysis

Raman spectroscopy can provide further insight into the structure of the sintered lines (presence of copper oxides) due to different Raman active vibrational modes. Figure 4, presents the Raman Spectra from the laser printed and sintered lines with increasing laser fluence (from 130 to 280 mJ/cm^2) and from printed lines dried in ambient atmosphere. Initially, all the lines are printed (lines of 90 μm width and 950 nm average height) in the same substrate and left to dry in atmosphere at room temperature. One of the printed lines is left unsintered and the rest are laser
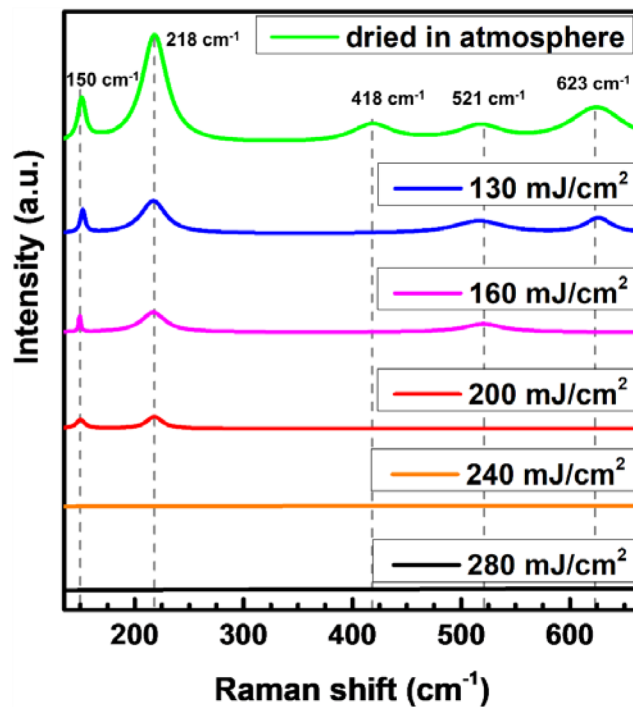

Fig. 4. Raman spectra of printed patterns dried in ambient atmosphere and sintered with increasing laser fluence

sintered with a single laser pass (without y-scanning) at different laser fluences. In more detail, the spectrum of the dried line in ambient atmosphere exhibited peaks at 150/218/418/521/623 cm^{-1}, which are assigned to Cu_2O peaks [45–46]. Raman spectra containing Cu_2O peaks have also been recorded for the sintered lines with laser fluence from 130 to 200 mJ/cm^2 (Table 1). It is observed in Fig. 4, that the dry patterns exhibit the most intense peaks we can obtain (they contain the higher amount of copper oxide), and the oxide peaks intensity decreases with increasing laser fluence. This indicates that the sintered lines with laser fluence of 240 and 280 mJ/cm^2, for which no peaks are detectable, are oxide free (any amount of copper oxide that may remain after sintering, is insignificant). The latter argument is further supported by the fact that resistivity takes its lowest value for 290 mJ/cm^2. Likewise, the EDX spectra (which can be found in Fig. 7, Appendix) of the sintered line with laser fluence at 280 mJ/cm^2 and the dried in atmosphere line respectively, indicate that the presence of oxygen in the sintered line is considerably lower than in the non-sintered line. Upon laser irradiation, the copper oxide is reduced to copper and the nanoparticles are subsequently sintered during a short period of time (laser pulse duration is about 100 ns). The reduction of Cu_2O to Cu has also been observed by Dharmadasa et al. [47] and Hwang et al. [21], who used intense pulse light to sinter Cu/Cu_2O nanoinks.

Table 1. Observed Raman Shifts of Copper Oxides from Fig. 4

Laser fluence (mJ/cm^2)	Peak (cm^{-1})					Compound
Dried in air	150	218	418	521	623	
130	150	218	-	521	623	
160	150	218	-	521	-	Cu_2O
200	150	218	-	-	-	
240	-	-	-	-	-	copper oxide free
280	-	-	-	-	-	

4. Test case: application in flexible circuit interconnection

The optimal sintering process parameters were applied for the additive manufacturing of a 5 loop conductive spiral trace fitting within an area of 3.6 mm x 3.6 mm.

Although the lowest resistivity was accomplished for a vertical overlap of 5 µm, the energy cost and the time duration of this process had to be considered, especially when aiming at the additive manufacturing of a large number of components, according to end-user requirements. Therefore, a calculation of the total deposited laser energy with respect to the vertical scanning step was carried out (Fig. 5 (left)). Taking into account the amount of energy and the time required for the sintering process, we selected the vertical scanning step of 25 µm, which is the most cost and time efficient trade-off between energy (~2 J), duration (~3.2 s) and resistivity (43 Ω). In this case, the resulting resistivity was ~ 5 µΩ·cm, when measured in short straight lines of 2 mm. However, in the actual spiral structure, with a total length of 40 mm micro-cracks, bulging and other minor structural defects may exist. These defects affect the overall electrical performance of this complicated geometry notably, resulting in a total resistance of 43 Ω, which would correspond to a resistivity with an average value of 17 µΩ·cm.

The displayed spiral structure shows an overall series resistance of <50 Ohms, a line width of 200 µm, line spacing 150 µm, and clean, sharp corner definition within these tolerances. This meets the design rule requirements for design and fabrication of a loop antenna, dedicated for a Near Field RFID system. In addition to meeting conductivity and pattern definition requirements, the ability to modify the printed pattern shape digitally via the laser-based process allows for a rapidly customizable on-chip antenna to meet varying market demands for low cost consumable tracking and other applications.
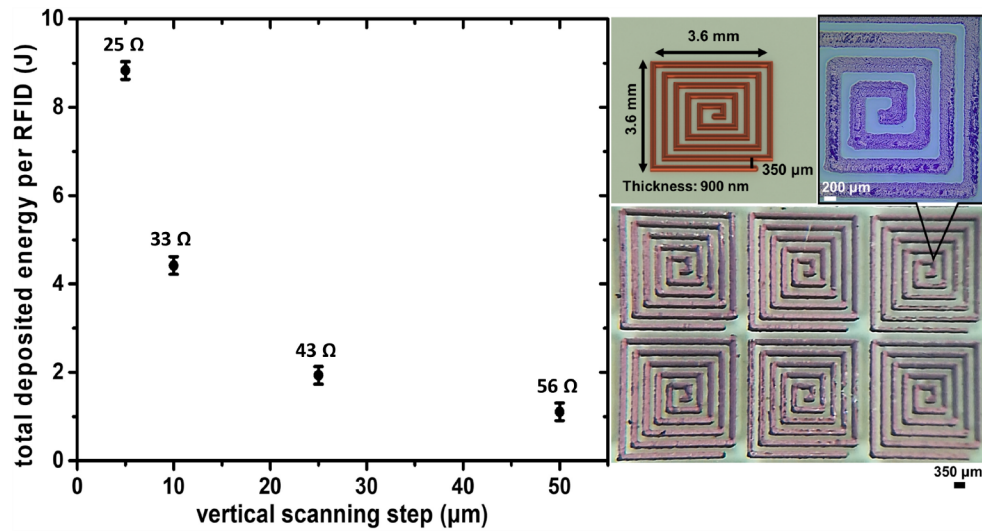
Fig. 5. Total deposited energy on the spiral pattern during sintering vs vertical scanning step (left), schematic illustration and optical microscopy photos (right). The total resistance decreases with decreasing scanning step.

5.　Summary

This work constitutes a successful demonstration of the combination of laser printing and laser sintering of Cu nanoparticle inks, for the fast and reproducible additive manufacturing of conductive patterns with design rules that enable the production of on-chip antennas on flexible integrated circuits. In particular, in this work, we have developed and synthesized a novel Cu nano-ink with properties optimized specifically for laser printing (high metal content 60%, high viscosity 430 kcP at 1 s^{-1}) and laser sintering (composition of additives and solvent). The laser printing process has been conducted in high speed (∼1 m/s), and the printed patterns were sufficiently reproducible, with a line width variation of about 5 μm. The laser sintering has been carried out effectively using the same set up as in printing, and the Cu nanoparticle patterns exhibit very low resistivity (3.3 μΩ·cm). The presence of copper oxide in sintered patterns decreases significantly after laser sintering and for sufficient laser fluence, the patterns are almost oxide free according to the Raman Spectra (and EDX spectra in the supplementary materials). The reported process can be readily employed for a variety of flexible Near Field RFID metallic components with form factors in the order of tens of micrometers up to centimeters and complex geometries, highlighting the advantages of laser additive manufacturing.
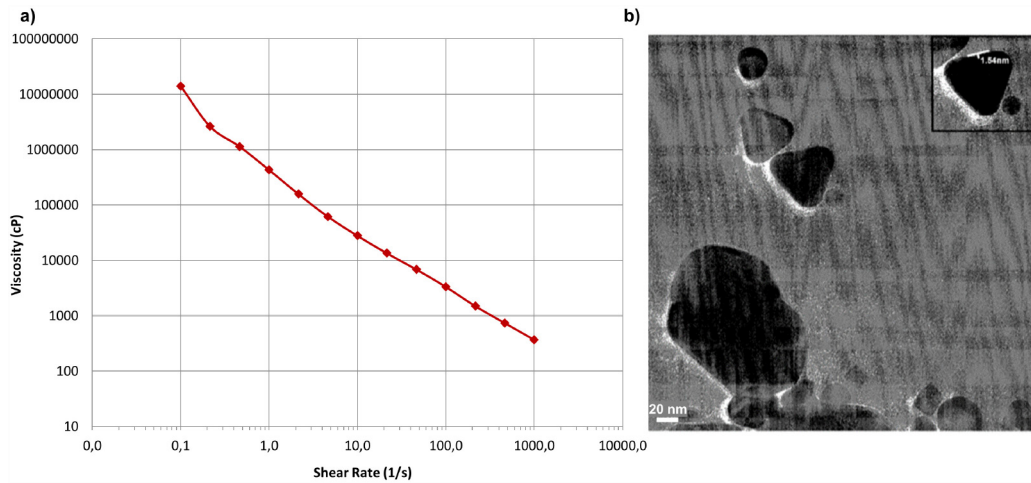
Appendix

Fig. 6. (a) Viscosity profile measurement of 60% Copper nanoparticle ink in DGBE solvent, and (b) TEM image of copper nanoparticles.
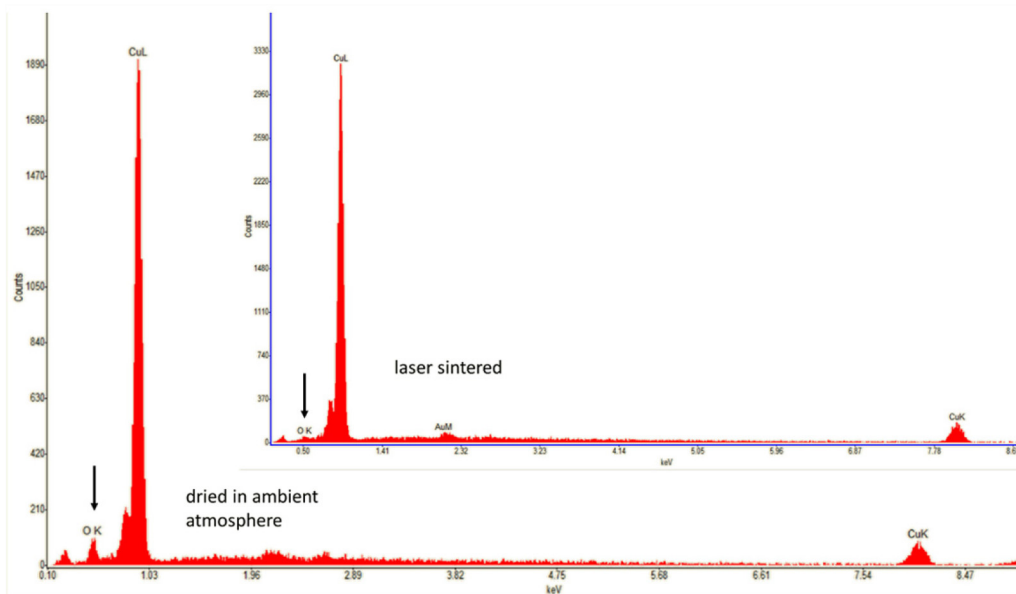

Fig. 7. EDX spectra of printed copper nanoparticle ink and dried in ambient air; Inset: EDX spectra of printed copper nanoparticle ink and laser sintered.

Funding

Acknowledgments

References

1. D. Li, W. Y. Lai, Y. Z. Zhang, and W. Huang, "Printable Transparent Conductive Films for Flexible Electronics," Adv. Mater. **30**(10), 1704738 (2018).
2. T. Han, A. Nag, N. Afsarimanesh, S. C. Mukhopadhyay, S. Kundu, and Y. Xu, "Laser-Assisted Printed Flexible Sensors: A Review," Sensors **19**(6), 1462 (2019).
3. A. Piqué, H. Kim, R. C. Y. Auyeung, I. Beniam, and E. Breckenfeld, "Laser-induced forward transfer (LIFT) of congruent voxels," Appl. Surf. Sci. **374**, 42–48 (2016).
4. E. Breckenfeld, H. Kim, R. C. Y. Auyeung, N. Charipar, P. Serra, and A. Piqué, "Laser-induced forward transfer of silver nanopaste for microwave interconnects," Appl. Surf. Sci. **331**, 254–261 (2015).
5. S. H. Ko, H. Pan, C. P. Grigoropoulos, C. K. Luscombe, J. M. Fréchet, and D. Poulikakos, "All-inkjet-printed flexible electronics fabrication on a polymer substrate by Low-dose laser sintering of Cu high-resolution selective laser sintering of metal nanoparticles," Nanotechnology **18**(34), 345202 (2007).
6. L. Rapp, E. Biver, A. P. Alloncle, and P. Delaporte, "High-Speed Laser Printing of Silver Nanoparticles Ink," J. Laser Micro/Nanoeng. **9**(1), 5–9 (2014).
7. R. C. Y. Auyeung, H. Kim, S. A. Mathews, and A. Piqué, "Laser Direct-Write of Metallic Nanoparticle Inks," J. Laser Micro/Nanoeng. **2**(1), 21–25 (2007).
8. M. Zenou, A. Sa'ar, and Z. Kotler, "Digital laser printing of aluminum microstructure on thermally sensitive substrates," J. Phys. D: Appl. Phys. **48**(20), 205303 (2015).
9. F. Zacharatos, M. Makrygianni, R. Geremia, E. Biver, D. Karnakis, S. Leyder, P. Puerto, P. Delaporte, and I. Zergioti, "Laser Direct Write micro-fabrication of large area electronics on flexible substrates," Appl. Surf. Sci. **374**, 117–123 (2016).
10. F. Zacharatos, P. Karvounis, I. Theodorakos, A. Hatziapostolou, and I. Zergioti, "Single Step Laser Transfer and Laser Curing of Ag NanoWires: A Digital Process for the Fabrication of Flexible and Transparent Microelectrodes," Materials **11**(6), 1036 (2018).
11. F. Zacharatos, I. Theodorakos, P. Karvounis, S. Tuohy, N. Braz, S. Melamed, A. Kabla, F. de la Vega, K. Andritsos, A. Hatziapostolou, D. Karnakis, and I. Zergioti, "Selective Laser Sintering of Laser Printed Ag Nanoparticle Micropatterns at High Repetition Rates," Materials **11**(11), 2142 (2018).
12. N. R. Bieri, J. Chung, S. E. Haferl, D. Poulikakos, and C. P. Grigoropoulos, "Microstructuring by printing and laser curing of nanoparticle solutions," Appl. Phys. Lett. **82**(20), 3529–3531 (2003).
13. B. K. Park, D. Kim, S. Jeong, J. Moon, and J. S. Kim, "Direct writing of copper conductive patterns by ink-jet printing," Thin Solid Films **515**(19), 7706–7711 (2007).
14. A. Yabuki and N. Arriffin, "Electrical conductivity of copper nanoparticle thin films annealed at low temperature," Thin Solid Films **518**(23), 7033–7037 (2010).
15. I. Kim and J. Kim, "The effect of reduction atmospheres on the sintering behaviors of inkjet-printed Cu interconnectors," J. Appl. Phys. **108**(10), 102807 (2010).
16. M. Joo, B. Lee, S. Jeong, and M. Lee, "Comparative studies on thermal and laser sintering for highly conductive Cu films printable on plastic substrate," Thin Solid Films **520**(7), 2878–2883 (2012).
17. F. Hermerschmidt, D. Burmeister, G. Ligorio, S. M. Pozov, R. Ward, S. A. Choulis, and E. J. W. List-Kratochvil, "Truly low temperature Sintering of printed copper ink using formic acid," Adv. Mater. Technol. **3**(12), 1800146 (2018).
18. J. Kwon, H. Cho, H. Eom, H. Lee, Y. D. Suh, H. Moon, J. Shin, S. Hong, and S. H. Ko, "Low-Temperature Oxidation-Free Selective Laser Sintering of Cu Nanoparticle Paste on a Polymer Substrate for the Flexible Touch Panel Applications," ACS Appl. Mater. Interfaces **8**(18), 11575–11582 (2016).
19. H. J. Hwang, W. H. Chung, and H. S. Kim, "In situ monitoring of flash-light sintering of copper nanoparticle ink for printed electronics," Nanotechnology **23**(48), 485205 (2012).
20. W. H. Chung, H. J. Hwang, and H. S. Kim, "Flash light sintered copper precursor/nanoparticle pattern with high electrical conductivity and low porosity for printed electronics," Thin Solid Films **580**, 61–70 (2015).
21. Y. T. Hwang, W. H. Chung, Y. R. Jang, and H. S. Kim, "Intensive plasmonic flash light sintering of copper nanoinks using a band-pass light filter for highly electrically conductive electrodes in printed electronics," ACS Appl. Mater. Interfaces **8**(13), 8591–8599 (2016).
22. Y. H. Son, J. Y. Jang, M. K. Kang, S. Ahn, and C. S. Lee, "Application of flash-light sintering method to flexible inkjet printing using anti-oxidant copper nanoparticles," Thin Solid Films **656**, 61–67 (2018).
23. H. S. Kim, S. R. Dhage, D. E. Shim, and H. T. Hahn, "Intense pulsed light sintering of copper nanoink for printed electronics," Appl. Phys. A **97**(4), 791–798 (2009).

24. I. Shishkovsky, V. Scherbakof, and I. Volyansky, "Low-dose laser sintering of Cu nanoparticles on the ceramic substrate during ink-let interconnection," *SPIE* 9065, 906501 (2013).

25. E. Halonen, E. Heinonen, and M. Mantysalo, "The effect of laser sintering process parameters on Cu nanoparticle ink in room conditions," Opt. Photonics J. **03**(04), 40–44 (2013).

26. E. Georgiou, S. A. Choulis, F. Hermerschmidt, S. M. Pozov, I. Burgues-Ceballos, C. Christodoulou, G. Schider, S. Kreissl, R. Ward, E. J. W. List-Kratochvil, and C. Boeffel, "Printed copper nanoparticle metal grids for cost-effective ITO-free solution processed solar cells," Sol. RRL **2**(3), 1700192 (2018).

27. C. W. Cheng and J. K. Chen, "Femtosecond laser sintering of copper nanoparticles," Appl. Phys. A **122**(4), 289 (2016).

28. N. Roy, J. Jeong, W. Jou, Y. Wang, H. Feng, and M. Cullinan, "Laser sintering of copper nanoparticles: a simplified model for fluence estimation and validation," proceedings of ASME, MSEC2017-2975 (2017).

29. H. Min, B. Lee, S. Jeong, and M. Lee, "Fabrication of 10 μm-scale conductive Cu patterns by selective laser sintering of Cu complex ink," Opt. Laser Technol. **88**, 128–133 (2017).

30. M. Zenou, O. Ermak, A. Saar, and Z. Kotler, "Laser sintering of copper nanoparticles," J. Phys. D: Appl. Phys. **47**(2), 025501 (2014).

31. J. Niittynen, E. Sowade, H. Kang, R. R. Baumann, and M. Mantysalo, "Comparison of laser and intense pulsed light sintering (IPL) for inkjet-printed copper nanoparticle layers," Sci. Rep. **5**(1), 8832 (2015).

32. http://intrinsiqmaterials.com/

33. http://www.italnanotech.com/

34. K. Myny, A. Tripathi, J. L. van der Steen, and B. Cobb, "Flexible thin-film NFC tags," IEEE Comm. Mag. **53**(10), 182–189 (2015).

35. B. Kim, S. Uno, and K. Nakazato, "Miniature on-chip spiral inductor RFID tag antenna fabricated with metal layer of standard CMOS process for biosensor applications," in *Proceedings of IEEE Topical Conf. Antennas and Propagation Wireless Communications*, 925-928 (2011).

36. J. Grosinger, W. Pachler, and W. Bosch, "Tag size matters: Miniaturized RFID tags to connect smart objects to the internet," IEEE Microw. Mag. **19**(6), 101–111 (2018).

37. A. Kalaitzis, M. Makrygianni, I. Theodorakos, A. Hatziapostolou, S. Melamed, A. Kabla, F. de la Vega, and I. Zergioti, "Jetting dynamics of Newtonian and non-Newtonian fluids via laser-induced forward transfer: Experimental and simulation studies," Appl. Surf. Sci. **465**, 136–142 (2019).

38. P. Abgrall, V. Conedera, H. Camon, A. M. Gue, and N. T. Nguyen, "SU-8 as astructural material for lab-on-chips and MEMS," Electrophoresis **28**(24), 4539–4551 (2007).

39. M. Makrygianni, I. Kalpyris, C. Boutopoulos, and I. Zergioti, "Laser induced forward transfer of Ag nanoparticles ink deposition and characterization," Appl. Surf. Sci. **297**, 40–44 (2014).

40. E. Biver, L. Rapp, A. P. Alloncle, P. Serra, and P. Delaporte, "High-speed multi-jets printing using laser forward transfer: time-resolved study of the ejection dynamics," Opt. Express **22**(14), 17122 (2014).

41. A. Palla-Papavlu, C. Córdoba, A. Patrascioiu, J. M. Fernández-Pradas, J. L. Morenza, and P. Serra, "Deposition and characterization of lines printed through laser-induced forward transfer," Appl. Phys. A **110**(4), 751–755 (2013).

42. I. Theodorakos, F. Zacharatos, R. Geremia, D. Karnakis, and I. Zergioti, "Selective laser sintering of Ag NPs ink for applications in flexible electronics," Appl. Surf. Sci. **336**, 157–162 (2015).

43. Engineering ToolBox, (2005). Thermal Conductivity of Metals, Metallic Elements and Alloys

44. P. B. Johnson and R. W. Christy, "Optical constants of the noble materials," Phys. Rev. B **6**(12), 4370–4379 (1972).

45. G. Niaura, "Surface-enhanced Raman spectroscopic observation of two kinds of absorbed OH- ions at copper electrode," Electrochim. Acta **45**(21), 3507–3519 (2000).

46. A. Singhal, M. R. Pai, R. Rao, K. T. Pillai, I. Lieberwirth, and A. K. Tyagi, "Copper(I) Oxide Nanocrystals – One Step Synthesis, Characterization, Formation Mechanism, and Photocatalytic Properties," Eur. J. Inorg. Chem. **2013**(14), 2640–2651 (2013).

47. R. Dharmadasa, M. Jha, D. A. Amos, and T. Druffel, "Room Temperature Synthesis of a Copper Ink for the Intense Pulsed Light Sintering of Conductive Copper Films," ACS Appl. Mater. Interfaces **5**(24), 13227–13234 (2013).